Major contribution of the 3/6/7 class of TRPC channels to myocardial ischemia/reperfusion and cellular hypoxia/reoxygenation injuries

Xiju He[a,b,c,1], Shoutian Li[a,b,1], Benju Liu[a,b], Sebastian Susperreguy[d], Karina Formoso[d], Jinghong Yao[e], Jinsong Kang[f], Anbing Shi[g], Lutz Birnbaumer[d,h,2], and Yanhong Liao[a,b,i,2]

[a]Department of Anatomy, Tongji Medical College, Huazhong University of Science and Technology, Wuhan, 430030, China; [b]Institute of Brain Research, Tongji Medical College, Huazhong University of Science and Technology, Wuhan, 430030, China; [c]Department of Anatomy, Hubei University of Medicine, Shiyan, 442000, China; [d]Institute of Biomedical Research (BIOMED), Catholic University of Argentina, Buenos Aires C1107AFF, Argentina; [e]Department of Infectious Disease, Union Hospital, Tongji Medical College, Huazhong University of Science and Technology, Wuhan, 430022, China; [f]Department of Surgery, Tongji Hospital, Tongji Medical College, Huazhong University of Science and Technology, Wuhan, 430030, China; [g]Department of Biochemistry and Molecular Biology, Tongji Medical College, Huazhong University of Science and Technology, Wuhan, 430030, China; [h]Neurobiology Laboratory, National Institute of Environmental Health Sciences, Research Triangle Park, NC 27709; and [i]Key Laboratory of Neurological Diseases of Ministry of Education, Tongji Medical College, Huazhong University of Science and Technology, Wuhan, 430030, China

Contributed by Lutz Birnbaumer, February 24, 2017 (sent for review December 28, 2016; reviewed by Thomas Gudermann and Eric N. Olson)

The injury phase after myocardial infarcts occurs during reperfusion and is a consequence of calcium release from internal stores combined with calcium entry, leading to cell death by apoptopic and necrotic processes. The mechanism(s) by which calcium enters cells has(ve) not been identified. Here, we identify canonical transient receptor potential channels (TRPC) 3 and 6 as the cation channels through which most of the damaging calcium enters cells to trigger their death, and we describe mechanisms activated during the injury phase. Working in vitro with H9c2 cardiomyoblasts subjected to 9-h hypoxia followed by 6-h reoxygenation (H/R), and analyzing changes occurring in areas-at-risk (AARs) of murine hearts subjected to a 30-min ischemia followed by 24-h reperfusion (I/R) protocol, we found: (*i*) that blocking TRPC with SKF96365 significantly ameliorated damage induced by H/R, including development of the mitochondrial permeability transition and proapoptotic changes in Bcl2/BAX ratios; and (*ii*) that AAR tissues had increased TUNEL$^+$ cells, augmented Bcl2/BAX ratios, and increased p(S240)NFATc3, p(S473) AKT, p(S9)GSK3β, and TRPC3 and -6 proteins, consistent with activation of a positive-feedback loop in which calcium entering through TRPCs activates calcineurin-mediated NFATc3-directed transcription of TRPC genes, leading to more Ca^{2+} entry. All these changes were markedly reduced in mice lacking TRPC3, -6, and -7. The changes caused by I/R in AAR tissues were matched by those seen after H/R in cardiomyoblasts in all aspects except for p-AKT and p-GSK3β, which were decreased after H/R in cardiomyoblasts instead of increased. TRPC should be promising targets for pharmacologic intervention after cardiac infarcts.

apoptosis | necrosis | calcium overload | calcineurin | AKT

Myocardial ischemia/reperfusion (I/R) injury is a major cause of morbidity and mortality in several important clinical scenarios, including acute myocardial infarction, cardiac arrest, percutaneous coronary artery intervention, and cardiac surgery. An abiding focus on time to reperfusion, i.e., when flow through the infarct-affected artery is reestablished either spontaneously or in response to therapeutic interventions, has proven critical for decreasing myocardial infarct size (IS) and preserving systolic function. This event, which restores oxygen and nutrients to the injured tissues, initiates a complex set of responses, globally referred to as "I/R injury," which lead to cell death preceded by inflammation, production of oxygen radicals, Ca^{2+} overload, and activation of mitochondrial apoptosis and necrosis (1). Myocardial Ca^{2+} overload induced by I/R is a major element of myocardial dysfunction in heart failure. Mitochondrial Ca^{2+} overload also can occur in cardiomyocytes as a consequence of ischemic stress during which aberrant intracellular Ca^{2+} is taken up by mitochondria. During I/R, Ca^{2+} accumulated in mitochondria leads to the activation of the mitochondrial permeability transition pore (mPTP) (2). Immediately after mPTP activation, mitochondria swell and release apoptogenic and necrogenic factors, which activate caspase-dependent and -independent cell death. Experimental animal studies have shown that pharmacologically inhibiting intracellular and mitochondrial calcium overload at the onset of myocardial reperfusion can reduce myocardial IS by 40–50% (3). However, clinical studies investigating this therapeutic approach have been disappointing thus far (4, 5), and pharmacologic intervention awaits the discovery of new drugs.

Given that mitochondrial Ca^{2+} overload is a leading cause of myocardial damage in I/R injury, reducing Ca^{2+} entry and cutting off the source of Ca^{2+} overload may prove an effective approach. Ca^{2+} handling by cells is orchestrated by a set of proteins, including the L-type calcium channel, sarco/endoplasmic reticulum Ca^{2+}-ATPase (SERCA pump), ryanodine receptor (RyR), sodium/calcium exchanger (NCX), and the mitochondrial calcium uniporter (MCU). Although attenuation of Ca^{2+} overload by targeting these proteins has provided cardioprotection in some settings of I/R (6, 7), clinical trials were limited by variables such as the effects of chronic inhibition of Ca^{2+} and the handling and timing of administration, calling for a better understanding of the regulatory mechanisms that govern Ca^{2+} handling by the heart.

Significance

Calcium overload has been recognized as a critical cause of the injury tissues suffer after periods of ischemia. The ports that determine calcium entry into tissues subjected to transient hypoxia have not been identified. Here we identify two members of the transient potential receptor channel (TRPC) family of nonselective cation channels that allow passage of calcium, TRPC3 and TRPC6, as major factors causing calcium entry in the heart, which is responsible for ischemia/reperfusion (I/R) injury. Blocking TRPC activity or the genetic ablation of TRPCs markedly protected cardiac tissue and cells from I/R injury. TRPC3 and TRPC6 are promising therapeutic targets.

Author contributions: X.H., S.L., L.B., and Y.L. designed research; X.H., S.L., B.L., S.S., K.F., J.Y., J.K., A.S., and Y.L. performed research; A.S. and L.B. contributed new reagents/analytic tools; X.H., S.L., B.L., S.S., J.Y., J.K., A.S., L.B., and Y.L. analyzed data; and X.H., S.L., K.F., L.B., and Y.L. wrote the paper.

Reviewers: T.G., Ludwig Maximilian University of Munich; and E.N.O., University of Texas Southwestern Medical Center.

The authors declare no conflict of interest.

[1]X.H. and S.L. contributed equally to this work.

[2]To whom correspondence may be addressed. Email: yhliao1@hust.edu.cn or Birnbau1@gmail.com.

This article contains supporting information online at www.pnas.org/lookup/suppl/doi:10.1073/pnas.1621384114/-/DCSupplemental.

Store-operated Ca entry (SOCE), also known as "capacitative calcium entry," is a major mechanism of Ca^{2+} entry existing in all cells, excitable and nonexcitable (8), which coexists with voltage-gated Ca^{2+} channels in neurons, skeletal muscle cells, and cardiomyocytes (9–12). Despite evidence that SOCE exists in cardiomyocytes, its acceptance as a contributor to cardiomyocyte Ca^{2+} homeostasis remains limited. Stromal interaction molecule 1 (STIM1) is now widely recognized as the molecular sensor of endoplasmic and sarcoplasmic reticulum Ca^{2+} and the trigger of SOCE. Orai1 (13–15) and canonical transient receptor potential channel (TRPC) proteins (16), including TRPC1 (17–19), TRPC4 (20, 21), and TRPC5 (22), have also been shown to play important roles in mediating SOCE, whereas TRPC3, TRPC6, and TRPC7 have been proposed, but not conclusively been proven to participate in the SOCE phenomenon, i.e., thapsigargin-evoked Ca^{2+} entry (23–25). TRPC proteins originate in seven genes coding for channel proteins (TRPC1–TRPC7) that are grouped into subfamilies by sequence and functional similarity: TRPC3, -6, and -7, which are activated by phospholipase C-generated diacylglycerols (DAGs); TRPC1, -4, and -5, of which TRPC1 is activated by STIM1 (19, 26); and TRPC2, which is expressed most highly in the vomeronasal organ of animals and is absent in *Homo sapiens* (27). During the last decade TRPC3 (28), TRPC4 (29), and TRPC6 (28) have been implicated in SOCE-mediated hypertrophic signaling in cardiomyocytes and in the initiation of pathologic cardiac remodeling (27, 30–32). TRPC channels are expressed at very low levels in normal adult cardiac myocytes, but the expression and activity of select isoforms appear to be increased in pathological hypertrophy and heart failure (30, 33). Transgenic cardiac-specific overexpression of TRPC3 or TRPC6 in mice causes reexpression of fetal genes, myocyte hypertrophy, and activation of apoptotic signaling (29, 34) leading Eder and Molkentin to conclude that "TRPC channels are bona fide regulators of cardiac hypertrophy associated with pathological events and neuroendocrine signaling" (27). In agreement, Makarewich et al. (35) found that Ca^{2+} influx through TRPC channels expressed after a myocardial infarct activates pathological cardiac hypertrophy and reduces contractility reserve. Blocking TRPC activity improved cardiac structure and function (35). To date, the roles of TRPCs in I/R injury have not been examined.

In the present study we tested the hypothesis that preventing a subset of DAG-activated TRPC channels from initiating their pathological activities in vivo would diminish I/R injury parameters in mice and, likewise, that inhibition of TRPC activity in vitro would diminish the damage initiated by hypoxia/reoxygenation (H/R) in murine cardiomyoblasts. Because there are no effective TRPC channel inhibitors for in vivo studies, we compared I/R injury in WT mice with that seen in triple-knockout mice lacking TRPC3, TRPC6, and TRPC7 (TRPC3/6/$7^{-/-}$ or TRPC3/6/7-KO mice).

Results

The initial finding that led us to investigate a possible role of TRPC channels in I/R injury was that SOCE evoked by the irreversible SERCA pump inhibitor thapsigargin was inhibited in H9c2 cardiomyoblasts (36) as well as in neonatal cardiomyocytes by 5 μM of the panTRPC inhibitor SKF96365 (Fig. 1 *A* and *B*), a concentration at which it does not affect bona fide Orai1-based Ca-release–activated Ca (CRAC) channels generated by the overexpression of inhibitory levels of Orai1 and rescuing levels of STIM1 (Fig. 1*G*) (37). The mouse heart expresses five of the seven TRPCs; TRPC5 and -7 are not expressed (Fig. 1*C*). The availability of TRPC3/6/$7^{-/-}$ triple-KO mice (Fig. 1*C*) led us to test whether the loss of these TRPCs had a quantitative effect on SOCE in their neonatal cardiomyocytes. As shown in Fig. 1 *E* and *F*, SOCE is diminished by about 60% in these triple-KO myocytes. Immunohistochemistry confirmed that cardiomyocytes from TRPC3/6/$7^{-/-}$ mice lack the C3 and C6 isoforms, confirming the specificity of the antibodies (Fig. 1*D*). It should be noted that higher concentrations of SKF96365 do inhibit Orai1-based SOCE (Fig. S1). Expression of Orai and STIM mRNAs was not affected by the disruption of the genes encoding TRPC3, -6, and -7 as seen in 35-cycle RT-PCR tests (Fig. S2).

SKF96365 Protects Against Changes Induced by H/R in the in Vitro H9c2 Myoblast Model of I/R Injury. The mitochondrial permeability transition (mPT), which results from the assembly of the mPTP and the collapse of the mitochondrial membrane potential (ψm), is one of the hallmarks of H/R injury. The presence of an assembled mPTP can be visualized in H9c2 myoblasts subjected to 9-h/6-h H/R by the change in fluorescence of the tetraethylbenzimidazolylcarbocyanine iodide (JC-1) reporter dye from red (JC-1 aggregated on the surface of polarized mitochondria) to green (JC-1 distributed as monomers in the cell). As shown in Fig. 2*A*, normoxic H9c2 cells stain red, whereas cells subjected to H/R stain green. The addition of SKF96365 during the H/R protocol inhibited the development of the mPT in a dose-dependent manner, suggesting that TRPC channels play a critical role in H/R injury. Note that significant protection was observed at 5 μM SKF96365, a concentration that does not affect Orai1-based Ca^{2+} entry channels. mPT is predictive of subsequent cellular apoptosis and necrosis (38), As shown in Fig. 1*B*, H9c2 cardiomyoblasts subjected to a 9-h/6-h H/R protocol have elevated levels of BAX (Bcl2-associated X protein), reduced levels of Bcl2 (B-cell lymphoma 2), and an increase in activated cleaved caspase 3. SKF96365 significantly ameliorated this picture of H/R injury (Fig. 2*B*). This protective effect was inhibited by the preaddition of the PI3K inhibitor LY294002 (Fig. 2*C*).

We next tested for changes in the levels of the serine/threonine protein kinase AKT phosphorylated at Ser473 [(p-Ser473)AKT], the activated form of AKT, which is a downstream target of PI3K, resulting from phosphorylation by phospholipid-dependent protein kinases (PDKs) and for changes in glycogen synthase kinase 3β (GSK3β) phosphorylated at Ser9 [(p-Ser9)GSK3β], an inactive form of GSK3β and a substrate of p-AKT. Both kinases were found to be partially activated, in sham-treated cells, and their activation (i.e., the level of the phosphorylated enzymes) was reduced by H/R. These H/R-induced changes were not only blocked by treatment of the cells with the TRPC inhibitor SKF96365 but were "reversed," in that the levels of the so-called "survival kinase" p-AKT and of p-GSK3β increased above the levels found in untreated cells (Fig. 2*C*). As occurred with BAX, Bcl2, and cleaved caspase 3 (Fig. 2*B*), the effects of H/R were blocked by 5 μM of the pan-TRPC inhibitor SKF96365, strongly suggesting that TRPC channels participate in the actions of H/R in these cells. As expected, preaddition of LY294002 prevented the activation of the PI3K signaling pathway.

We also tested whether H/R causes activation of nuclear factor of activated T cells, cytoplasmic 3 (NFATc3) resulting from dephosphorylation by the phosphoprotein phosphatase calcineurin (CaN), which in turn is activated by Ca^{2+}-calmodulin (CaM). Dephosphorylation of p-NFATc proteins exposes a nuclear localization signal (NLS) triggering the translocation of NFATc into the nucleus where it associates with nuclear NFAT (NFATn) or, depending on cellular context, with other transcription factors, including GATA binding proteins 3/4 (39), activator protein 1 (AP1) (40), and myocyte enhancer factor 2 (MEF-2) (41), and binds to consensus NFAT-binding sites to drive the transcription of NFAT target genes (42). We found that H/R causes a decrease in the levels of p-NFATc3, one of the four NFATc isoforms expressed in cardiomyocytes (Fig. 2*D*) (43), consistent with activation of the NFAT transcription pathway. SKF96365 (5 μM) prevented NFAT activation (Fig. 2*D*), again indicating the involvement of TRPC channels in Ca^{2+} influx. By an unknown mechanism H/R not only led to dephosphorylation of NFATc3 without significant changes in total NFATc3 levels (Fig. 2*D*) but also caused an increase in both CaN subunit proteins, CaNα and CaNβ (Fig. 2*E*).

The transcription of both TRPC3 and TRPC6 has been shown to be under the control of the NFAT transcription machinery. Conserved NFAT consensus sites have been found in the promoter of TRPC6 (31), and TRPC3 has been shown to be

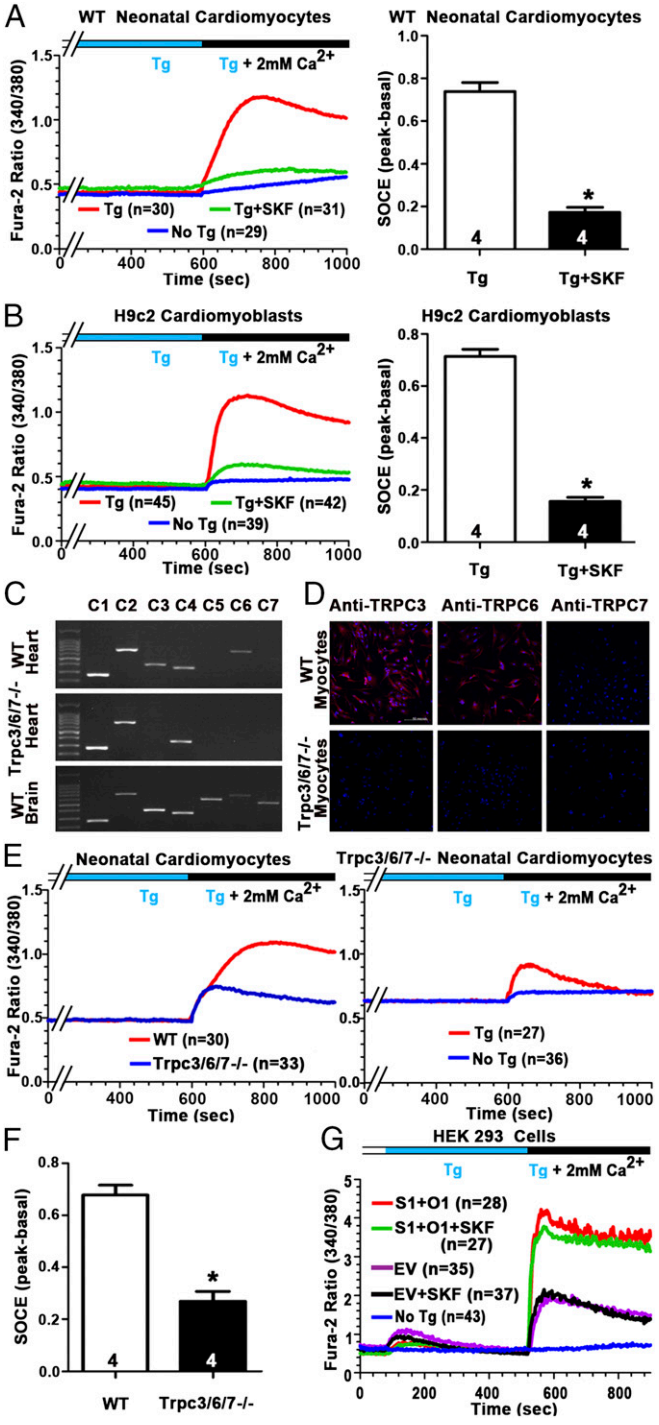

Fig. 1. A large proportion of the Ca^{2+} that enters cardiac cells after depletion of Ca^{2+} stores depends on channels formed by TRPC3 and/or TRPC6. (*A* and *B*) Inhibition of SOCE by 5 μM of the pan-TRPC inhibitor SKF96365 in neonatal cardiomyocytes (*A*) and in H9c2 cardiomyoblasts (*B*). (*Left*) Time course of $[Ca^{2+}]i$ changes as seen in Fura2-loaded cells. Traces are averages of the indicated number of cells. (*Right*) Summary results of peak intracellular Ca^{2+} concentrations reached in the Ca^{2+} entry phase of the SOCE assays (means ± SEM of the indicated number of experiments; $*P < 0.05$). (*C*) Expression of TRPC mRNAs in cardiac ventricles as seen by 35-cycle RT-PCR analysis. (*Top*) Five of the seven TRPCs are expressed in the myocardium. (*Middle*) TRPC5 and -7 mRNAs are undetectable in ventricles of Trpc3/6/7$^{-/-}$ mice. (*Bottom*) All TRPC mRNAs are detected in whole brains of WT mice (positive controls). (*D*, *Upper*) Immunohistochemistry analysis shows the presence of TRPC3 and TRPC6 but not TRPC7 proteins in neonatal cardiomyocytes of WT mice. (*Lower*) TRPC3 and TRPC6 proteins are undetectable in neonatal cardiomyocytes of TRPC3/6/7$^{-/-}$ mice. (Magnification: 20×.) (*E*) Reduction of SOCE in neonatal cardiomyocytes from TRRPC3/6/7$^{-/-}$ mice. (*Left*) Comparison of SOCE in WT cells and in TRPC3/6/7$^{-/-}$ cells. (*Right*) SOCE in TRPC3/6/7$^{-/-}$ cells. (*F*) Summary of peak SOCE values in WT and TRPC3/6/7$^{-/-}$ cells. Data are shown as the means + SEM of the indicated number of independent experiments; $*P < 0.05$. (*G*) SKF96365 (SKF) at 5 μM does not inhibit Orai1-based SOCE in HEK293 cells. SOCE was evoked in HEK293 cells cotransfected with empty vectors (EV) or with vectors coding for Orai1 (O1) and STIM1 (S1), as indicated, loaded with Fura-2, and monitored for intracellular Ca^{2+} changes evoked by 2 μg/mL thapsigargin. Traces are averages of the changes observed in the indicated number of cells. Tg, thapsigargin.

up-regulated in an NFAT-dependent manner upon exercise in skeletal muscle (44). Because H/R causes activation of this transcription machinery, we examined whether H/R was associated with increases in TRPC3 and TRPC6 proteins in H9c2 cells. As shown in Fig. 3*A*, TRPC3 and TRPC6 protein levels were elevated in H9c2 cardiomyoblasts after H/R, and this change was accompanied by a functional correlate of TRPC3 and TRPC6 protein levels: increased Ca^{2+} influx in response to the TRPC3/6/7 agonist oleyl-acetyl-glycerol (OAG) (Fig. 3*B*). The H/R-induced increase in DAG-stimulated Ca^{2+} entry was inhibited by 5 μM SKF96365 (Fig. 3*B*), which is consistent with the idea that the increase is indeed caused by an increase in the I/R-induced expression of functional DAG-sensitive TRPC channels of the TRPC3 and TRPC6 type.

To gain insight into whether the H/R-induced up-regulation of TRPC channels also occurs in vivo in murine hearts subjected to an I/R protocol, we examined the effect of I/R on tissues from cardiac areas at risk (AAR), the areas that had suffered loss of blood supply for 30 min and then had been reirrigated when the arterial occlusion was removed for 24 h and that had not died in this time period. Changes in these areas are assumed to be those that precede future tissue death. As illustrated in Fig. 3*C*, and as expected, TRPC3 and TRPC6 protein levels were increased in the AARs of WT mice subjected to I/R but not in the AARs of TRPC3/6/7$^{-/-}$ mice (Fig. 2*D*). As can be seen, the Western blots of the AAR tissue from TRPC3/6/7-KO mice were not blank: They showed weak bands that migrate at the same level as the bands from WT mice that increased in intensity upon I/R. We consider these bands to be nonspecific, because they did not change upon I/R in step with the bands we interpret as TRPC3 and TRPC6 proteins (Fig. S3). Weak bands of this type were present in TRPC3/6/7$^{-/-}$ tissues when we used the antibodies given to us by Veit Flockerzi from the University of the Saarland, Saarbrücken, Germany and also when we used several commercial antibodies, including those used for immunohistochemistry in Fig. 1*D*. Levels of another TRPC, TRPC4, were unaffected by I/R (Fig. 3*E*).

TRPC3/6/7-KO Mice Are Significantly Protected from I/R Injury. IS is substantially reduced in TRPC3/6/7-KO mice exposed to 30 min of cardiac ischemia and 24 h of reperfusion as compared with WT mice subjected to the same treatment (IS, 24.4 ± 2.3% vs. 44.1 ± 3.5%; $n = 12$; $P < 0.05$) (Fig. 3*A*). There was no significant difference in the AAR in the two groups (52.6 ± 2.6% vs. 50.5 ± 2.1% AAR; $n = 12$) (Fig. 3*A*), confirming that the surgical injury was equivalent in the treatment groups. WT and TRPC3/6/7-KO mice show no differences in preocclusion hemodynamics (heart rate, mean arterial pressure, and rate-pressure product).

After 30 min of ischemia and 24 h of reperfusion, the cardiac functions of TRPC3/6/7-KO mice, as measured by transmural echocardiography, were less impaired than those of WT mice (Fig. 4*B*). Both the ejection fraction (EF) (sham treatment vs. I/R: 79.8 ± 2.5% vs. 36.5 ± 2.2%) and fractional shortening (FS) (sham treatment vs. I/R: 46.1 ± 3.0% vs. 19.5 ± 2.1%, $n = 8$) were reduced after I/R in WT mice, as were the EF (sham treatment vs. I/R: 78.7 ± 2.0% vs. 56.8 ± 3.3); and FS (sham treatment vs. I/R: 44.5 ± 3.4% vs. 30.7 ± 2.5%, $n = 8$) in TRPC3/6/7$^{-/-}$ mice. However, the degree of functional loss was significantly less in

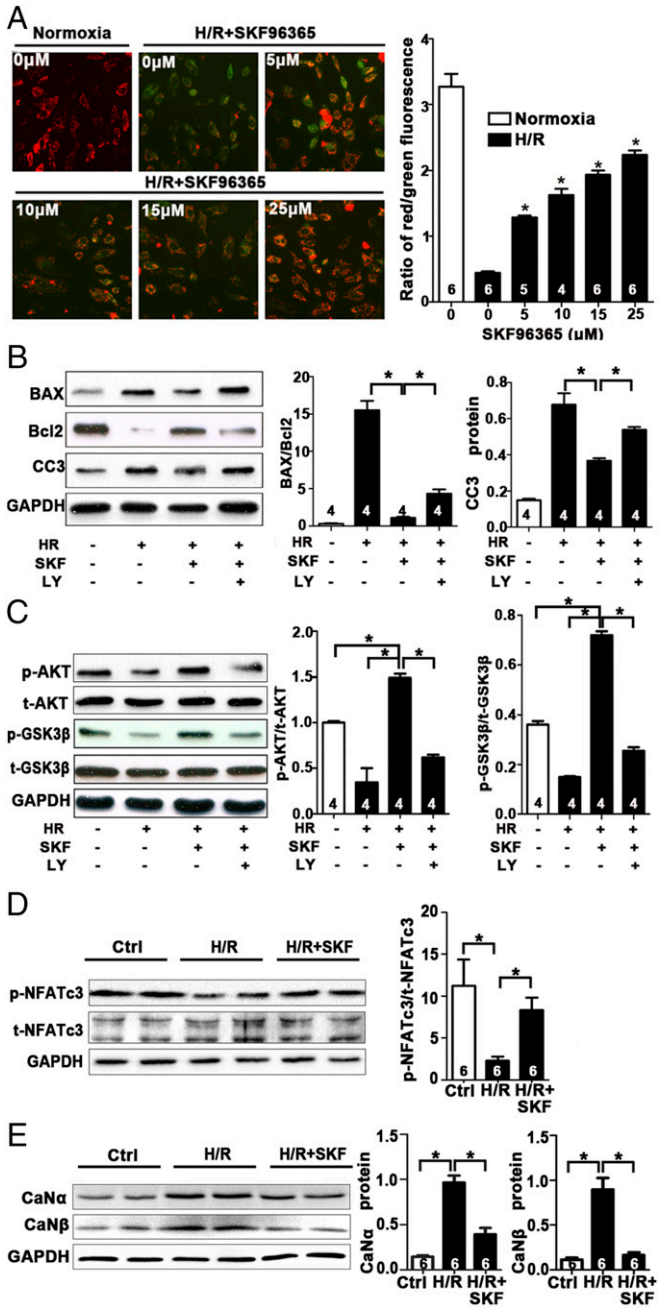

Fig. 2. The pan-TRPC inhibitor SKF96365 significantly protects H9c2 cardiomyoblasts against H/R injury. H/R effects depend on decreased PI3K activity. (*A*, *Left*) mPT (JC-1 red to green stain) after the H/R procedure is largely prevented by increasing concentrations of SKF96365. (*Right*) Ratios of red/green cells. Shown are means ± SEM; $*P < 0.05$ from the indicated number of experiments. (*B–E*) Western blot analyses of changes in the levels of the indicated proteins in H/R-treated H9c2 cardiomyoblasts (*Left*) and bar graphs depicting summary averages of the indicated number of experiments of the observed changes (*Right*). Values are means ± SEM; $*P < 0.05$. (*B*) Changes in Bcl2, BAX, and cleaved caspase 3 (CC3) proteins in H/R-treated cells; the protective effect of 5 μM SKF96365 (SKF) and the failure of protection when the PI3K inhibitor LY294002 is present during the H/R procedure are seen. (*C*) Changes in p-AKT, t-AKT, p-GSK3β, and t-GSK3β proteins in H/R-treated cells and inhibition of the changes induced by H/R by the presence of 5 μM SKF96365. Inhibition of PI3K by 30 μM LY294002 is dominant. (*D*) Changes in (p-Ser240)NFATc3 levels upon H/R treatment and the prevention of these changes by 5 μM SKF96365. (*E*) Up-regulation of CaNα and CaNβ subunit levels by H/R treatment. ns, not significant. Ctrl, control.

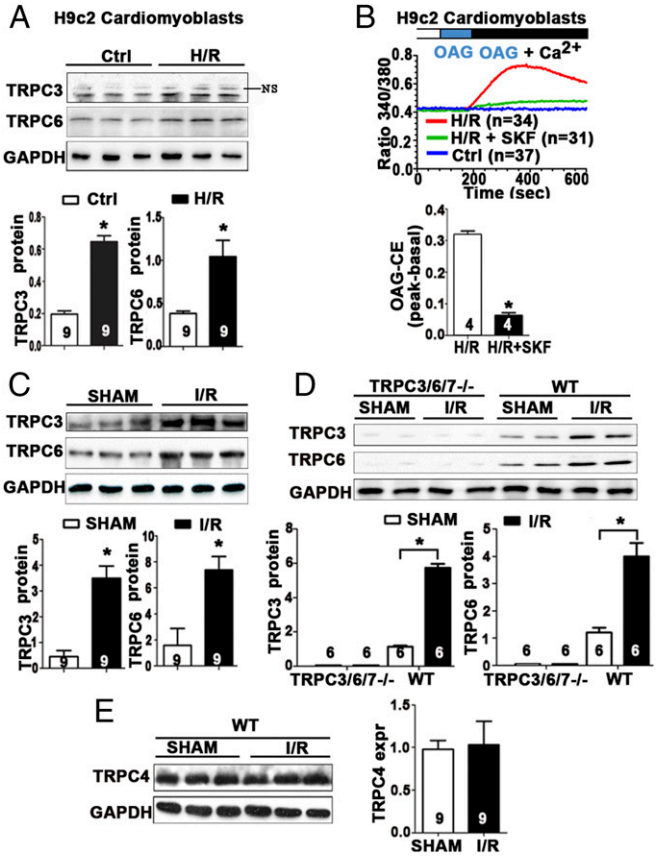

Fig. 3. H/R in vitro and I/R in vivo up-regulate TRPC3 and TRPC6 channel proteins. Each lane is the blot of an independent cell or mouse tissue sample. Bar graphs show summary averages of the indicated number of independent experiments. Data are shown as means ± SEM; $*P < 0.05$ for all panels. (*A*) H/R treatment of H9c2 cardiomyoblasts leads to increased TRPC3 and TRPC6 protein levels. (*B*) Increased OAG-stimulated Ca^{2+} entry in response to H/R treatment in H9c2 cardiomyoblasts. The OAG-stimulated Ca^{2+} entry is inhibited by 5 μM SKF96365 (SKF). (*C* and *D*) Western blot analyses of TRPC3 and TRPC6 levels in AAR regions of WT and TRPC3/6/$7^{-/-}$ hearts from mice subjected to the I/R procedure or in ventricles of sham-operated mice, showing increased TRPC3 and TRPC6 proteins after I/R (*C* and *D*) and the absence of TRPC3 and TRPC6 immunoreactivity in the corresponding samples from TRPC3/6/$7^{-/-}$ tissues (*D*), proving antibody specificity. (*E*) TRPC4 protein levels are unaffected by I/R. Ctrl, control.

TRPC3/6/$7^{-/-}$ mice than in WT mice (Fig. 4*B*, summary bar graphs). These data revealed that TRPC channels contribute significantly to I/R injury, as seen by the amelioration of damage in TRPC3/6/$7^{-/-}$ mice.

Fig. 4*C* presents the results of histological examination of the AAR in left ventricle myocardial tissues in different groups. Compared with the sham-treated group, distinct alterations occurred in the AAR after I/R, including disruption of myocardial fibers, tissue edema, and neutrophil infiltration. Fig. 4*C* illustrates the disruption of myocardial fibers (arrow *a*), neutrophil infiltration (arrow *b*), and tissue edema (arrow *c*). Of note, all the I/R-induced alterations were ameliorated in TRPC3/6/7-KO mice.

To determine whether TRPC3/6/7-KO mice have preserved ultrastructure after I/R injury, cardiac tissues were examined by transmission electron microscopy. Control cardiomyocytes in tissues from both WT and TRPC3/6/7-KO mice had well-arranged sarcomeres and intercalated discs and also had normal mitochondria without signs of swelling, intact cristae density, and other ultrastructures (Fig. 4*D*). However, I/R injury in WT mice resulted in marked ultrastructural damages recognized by absent and unclear sarcomeres and degenerative alterations of myofilaments.

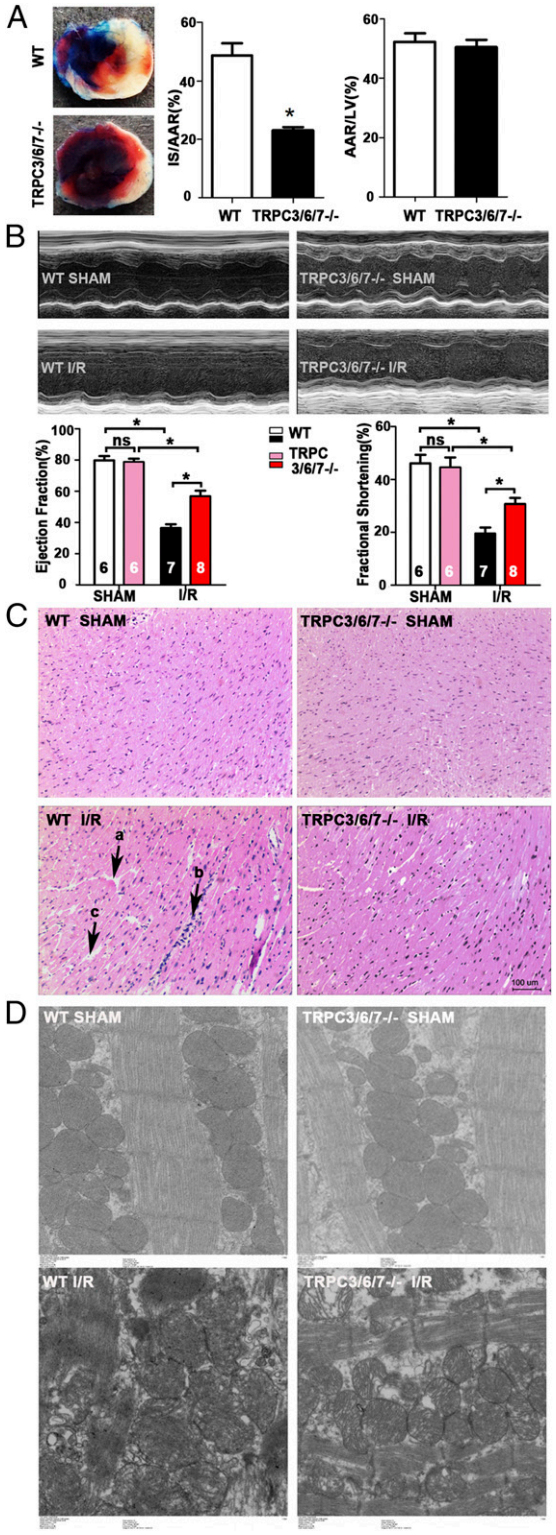

Fig. 4. Ameliorated I/R injury in TRPC3/6/7$^{-/-}$ mice. (*A*) Evans blue-TTC staining of ∼1-mm-thick heart slices from a TRPC3/6/7$^{-/-}$ mouse and a WT mouse after 30-min/24-h I/R. White indicates infarct; red indicates the AAR; and blue indicates the area not subjected to blood supply interruption. TRPC3/6/7$^{-/-}$ mouse hearts have reduced IS normalized to AAR+IS ($n = 11$, $^*P < 0.05$) as determined by TTC staining after I/R. There were no significant differences in AAR between groups. (Magnification: 12×.) (*B*) A representative echocardiograph recorded from a mouse after 30-min/24-h I/R. Representative M-mode tracings from sham- and I/R-treated animals are shown. Average cardiac EF and left ventricular FS were computed. TRPC3/6/7$^{-/-}$ mice partially preserved FS and EF after I/R injury ($n = 7$; $^*P < 0.05$; ns, not significant). (*C*) Representative H&E-stained histological images of the AAR of left ventricle myocardial tissues in different groups. The image at the lower left shows the presence of disrupted myocardial fibers (arrow *a*), the presence of infiltrated neutrophils (arrow *b*), and edema (arrow *c*) in AARs of WT mice after I/R; TRPC3/6/7$^{-/-}$ hearts had a less damaged myocardium after I/R. (Scale bar: 100 μm.) (*D*) Electron micrograph of AARs from the hearts of WT and TRPC3/6/7$^{-/-}$ mice after I/R. No tissue swelling or structural changes were seen in sham-treated WT and TRPC3/6/7$^{-/-}$ mice. Unclear sarcomeres, degenerative alterations of myofilament, and fusion and disruption of the mitochondrial cristae were observed in WT mice after I/R injury. TRPC3/6/7$^{-/-}$ mice had fewer damaged myocytes and mitochondria after I/R. (Magnification: 5,000×.)

Additionally, fusion and vacuolation of mitochondria with pronounced derangement and disruption of mitochondrial membranes and cristae were observed in the I/R group. All the I/R-induced ultrastructure alterations seen in WT mice were ameliorated in TRPC3/6/7-KO mice (Fig 4*D*).

Reduced Apoptosis After I/R in TRPC3/6/7$^{-/-}$ Mice Through Inhibition of the CaN–NFAT Signaling Path and Up-Regulation of the PI3K–AKT–GSK3β Survival Signaling Pathway. We next sought to obtain information indicating that the cellular changes observed in the in vitro I/R models had in vivo correlates by analyzing changes that occur in the AARs of the ventricles of TRPC3/6/7$^{-/-}$ mice subjected to I/R.

Changes in proapoptotic BAX and antiapoptotic Bcl2 levels upon H/R predicted that the level of apoptosis in AAR tissues should be less in TRPC3/6/7$^{-/-}$ mice than in WT mice, and, indeed, we observed this difference in vivo (Fig. 5*A*). Thus, TRPC3/6/7-KO mice had reduced apoptosis, as seen in TUNEL$^+$ cells (apoptotic rate, 19.2 ± 2.1% in TRPC3/6/7-KO mice vs. 45.8 ± 2.9% in WT mice; $n = 10$; $P < 0.05$). Proapoptotic signaling, i.e., BAX/Bcl2 ratios and cleaved caspase 3, was augmented upon I/R and was ameliorated in TRPC3/6/7$^{-/-}$ AARs (Fig. 4*B*). Likewise, survival signaling, e.g., p-AKT and p-GSK3β, was significantly increased after I/R in TRPC3/6/7$^{-/-}$ AARs compared with WT AARs (Fig. 5*C*). As shown in Fig. 5*D*, similar to our findings in H9c2 cardiomyoblasts (Fig. 2*D*), p-NFATc3 levels were significantly decreased in the AAR tissue of WT mice subjected to I/R. This effect was markedly ameliorated in TRPC3/6/7$^{-/-}$ mice. An examination of the protein levels of the two subunits that make up the Ca^{2+}/CaM-dependent calcineurin enzyme revealed that the levels of both CaNα and CaNβ are augmented in the AAR tissues of mice subjected to I/R compared with their levels in left ventricular tissue of sham-operated mice (Fig. 5 *E*, *i*). This increase in phosphatase protein subunits did not occur in the AAR tissue from TRPC3/6/7$^{-/-}$ mice; on the contrary, CaNα and CaNβ protein levels were lower in the AAR tissue of TRPC3/6/7$^{-/-}$ mice than in the AAR tissue of WT mice (Fig. 5 *E*, *iii*). This difference was not the result of an independent consequence of the TRPC gene disruption, because CaN protein levels in sham-operated WT and TRPC3/6/7$^{-/-}$ mice were indistinguishable (Fig. 5 *E*, *ii*).

The CaM–CaN–NFAT pathway plays a crucial role in cardiac hypertrophy (45) and in other tissues, including skeletal muscle (44). In the present studies it seems likely that NFATc3 is at least partly responsible for the up-regulation of TRPC3 and -6 channels in cardiomyoblasts subjected to H/R, because H/R led to partial dephosphorylation of p-NFATc3 (Fig. 2*D*), and for the up-regulation of TRPC3 and TRPC6 (Fig. 3 *A* and *B*). In an attempt to gain an independent view on the NFAT dependence of the up-regulation of TRPC3 and TRPC6 channels, as well that of BAX (Fig. 2*B*) seen upon H/R, we exposed H9c2 cardiomyoblasts to H/R in the absence and presence of the cell-permeable inhibitor of p-NFAT dephosphorylation, 11R-VIVIT (46). As shown in Fig. 5*F*, inhibition of p-NFATc dephosphorylation without inhibition of CaN activity, by preventing access of CaN to the p-NFAT molecule, prevented the up-regulation of TRPC3, TRPC6, and BAX observed upon H/R treatment of the H9c2 cardiomyoblasts.

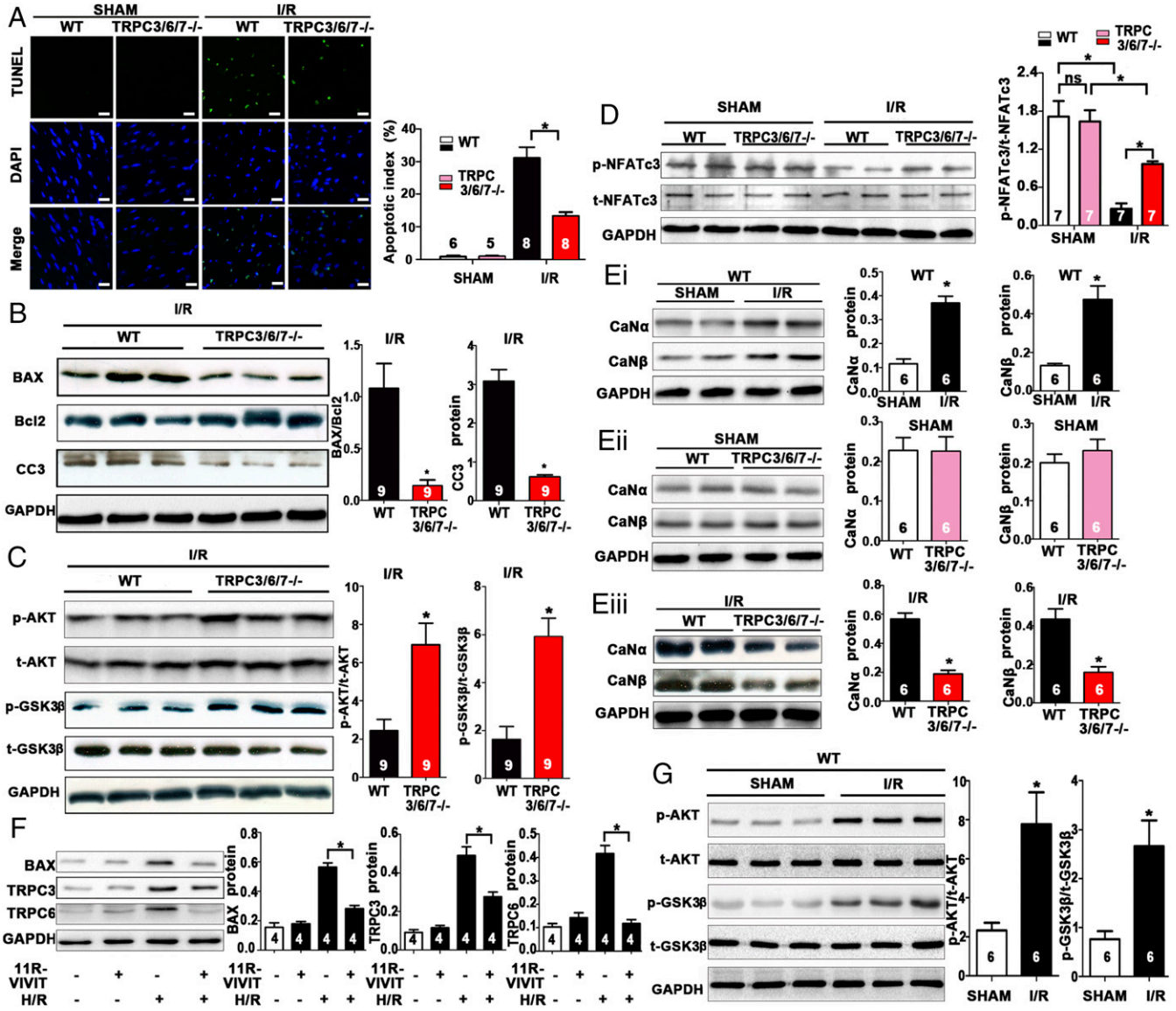

Fig. 5. Injury caused in vivo by I/R involves a positive-feedback loop mediated by NFATc3's transcription of *BAX* and *TRPC* genes and is ameliorated by the ablation of TRPC3 and TRPC6. (*A–E*) Analysis of AARs after I/R showed that, as compared with WT mice, TRPC3/6/7$^{-/-}$ mice had a decreased proportion of cells undergoing apoptosis (*A*) and, as seen by Western blotting (*B–E*), had decreased levels of the proapoptotic markers BAX and cleaved caspase 3 (CC3) and increased levels of antiapoptotic Bcl2 (*B*); improved levels of survival signaling markers p-AKT and p-GSK3β (*C*); lower levels of activated p-NFATc3 (*D*); and lower levels of CaNα and CaNβ subunit proteins (*E*, *i–E*, *iii*). (Scale bars: 40 μm.) (*F*) I/R-activated NFATc drives the expression of I/R-induced BAX, TRPC3, and TRPC6. (G) I/R caused p-AKT and p-GSK3β proteins to increase reflecting activation of the PI3K-signaling pathway. In the Western blot images in all panels, each lane is the blot of an independent cell or mouse tissue sample. Values are means ± SEM of the indicated number of experiments. *$P < 0.05$; ns, not significant.

Discussion

The studies presented here have examined the impact of a DAG-activated subclass of TRPC channels, TRPC3, -6, and -7, on the consequences of I/R in vivo, as they affect key mediators of the injury phase of I/R injury. We present a parallel set of studies in which the effects of H/R, as seen in an in vitro cell model (H9c2 cardiomyoblasts) are compared with findings seen in vivo in cardiac I/R experiments in mice.

In both systems we found that blocking TRPC channel activity in vitro had the same effects on H/R-induced changes as the genetic ablation of the TRPC3 and TRPC6 channels had on I/R-induced changes. Thus, preventing TRPC channel function increased the levels of p-AKT and p-GSK3β, increased protein levels of anti-apoptotic Bcl2, and at the same time decreased levels of BAX, one of the components of the mitochondrial apoptosis-induced channel (MAC) through which cytochrome *c* exits to precipitate mitochondrial apoptosis (47). Blocking TRPC function also reduced H/R- and I/R-induced cleaved caspase 3 (Fig. 5 *C* and *E*). Interestingly, protein levels of TRPC3 and TRPC6 increased upon H/R and I/R (Fig. 2 *A* and *C*), as did protein levels of the CaNα and CaNβ subunits of CaN (Figs. 2 and 5 *E*, *i*); the last is in agreement with a prior report (48), but the mechanism (increased transcription/synthesis or diminished protein degradation) is unknown to us.

Our experiments revealed a significant difference in the effect of H/R in cardiomyoblasts and I/R in AAR tissue: H/R resulted in a decrease in p-AKT and p-GSK3β (Fig. 2*C*), whereas I/R, as seen in the AAR tissue, increased p-AKT and p-GSK3β (Fig. 5*G*). Because (p-Ser9)-GSK3β is a reflection of (p-Ser473)-AKT activity, and p-AKT is a reflection of PI3K activity, the difference is counterintuitive and puzzling. The cardiomyoblasts responded by reducing their PI3K activity, creating a proapoptotic environment,

whereas AAR tissues responded by increasing PI3K activity, creating a less apoptotic environment than exists in sham-operated ventricle muscle. Biochemical explanations exist for both types of response.

The mechanism responsible for decreased PI3K activity could lie in an hypoxia-induced transcription of PI3K-interacting protein 1 (PIK3IP1) found in cultured cardiac cells (49). PIK3IP1 is a glycosylated membrane protein with similarity to the PI3K p85 regulatory subunit and inhibits PI3K (50). The proapoptotic environment created by reduced PI3K activity is exploited during the reoxygenation phase of the H/R procedure to trigger a proapoptotic program initiated by reactive oxygen generated by plasma membrane-resident NADPH oxidase isoform 2 (Nox2), possibly facilitated by the recently described stretch-induced, TRPC3-dependent activation of Nox2, the stretch signal being provided by the known effect of hypoxia in promoting cell swelling (51). Although not directly assessed, because the decrease in p-AKT is blocked by the PI3K inhibitor LY294002 (30 μM), we surmise that the decrease in p-AKT is caused by a decrease in PI3K activity. Reactive oxygen species (ROS) generated during the reoxygenation phase then would activate Bcl2-associated death promoter (Bad), a member of the BH3-only family of Bcl2 proteins, likely causing Bad, which is expressed in cardiomyocytes, to trigger apoptosis by sequestering Bcl2 away from the proapoptotic BAX. The decrease in PI3kinase activity upon H/R in H9c2 cells is supported by the decrease in p-AKT activity reflected in decreased p-GSK3β levels, but direct examination of PIK3IP1 mRNA changes by 35-cycle RT-PCR did not support this hypothesis, because PIK3IP1 mRNA levels increased instead of decreasing (Fig. S4*B*).

On the other hand, the mechanism responsible for activation of PI3K in AAR tissues may be triggered by activation of TRPC6 during the hypoxia phase of the I/R process, akin to the mechanism by which endothelial cell activation of TRPC6 by LysoPC (1-palmitoyl-sn-glycero-3-phosphocholine) activates PI3K in a Ca^{2+}-CaM–dependent manner. In endothelial cells activation of TRPC6 results in release of TRPC6-resident CaM, which migrates to nearby PI3K where it interacts with the p85 regulatory subunit, stimulating the activity of the p110 catalytic subunit to generate PIP3 from PIP2 (52). Activation of PI3K by Ca-CaM has been described (53). Activation of PI3K upon I/R treatment was facilitated further by an accompanying decrease in mRNA levels of PIK3IP1 and a concomitant decrease in its protein levels (Fig. S4*A*). These reactions eventually led to increased, functionally active p-AKT, as evidenced by the increase in p-GSK3β (Fig. 5*G*). Although the increase p-AKT in AAR tissue became apparent in experiments that included 24 h of reperfusion, the increase was independent of the reperfusion phase, because it was apparent before the reperfusion phase of the protocol (Fig. S5).

p-AKT is antiapoptotic by virtue of its actions in phosphorylating Bad on Ser155, which prevents it from sequestering Bcl2 away from BAX (54, 55), and in phosphorylating BAX on Ser184, increasing its affinity for Bcl2 (56) and thus interfering with BAX oligomerization and assembly into the MAC channel in the mitochondrial outer membrane (MOM). A reasonable scenario that would bring H/R and I/R changes into register is that in the I/R situation the increases in p-AKT activity are far from maximal, because ablation of TRPC3/6/7 led to further large increases in p-AKT and p-GSK3β (Fig. 5*C*), and that, on the whole, apoptotic plus necrotic death signals outweigh the weak antiapoptotic activity generated by I/R.

However, the difference between the H9c2 response and the AAR response may reside in the fact that H9c2 cells are myoblasts (36), not bona fide cardiomyocytes. Wang et al. (57), working with fresh neonatal rat cardiomyocytes, reported that H/R leads to an increase in p-AKT akin to the increase we saw in AAR tissues after I/R.

In both cases, the overriding result of H/R in cardiomyoblasts and of I/R in ventricle tissue appears to be a combination of apoptosis and necrosis. The latter is triggered by the development of mPT as a result of the assembly of the mPTP (Fig. 2*A*). The mPT begins with the assembly of the mPTP and collapse of the inner ψm and continues with swelling and rupture of the outer membrane and the release of proteins, generation of large amounts of ROS, and death of the cell by necrosis. An important intermediary step is the massive entry of Ca^{2+} into the matrix carried not only by mitochondrial Ca^{2+} uniporter (MCU) but also by a fraction of TRPC3 embedded in the inner mitochondrial membrane and functioning in parallel with MCU (58). Our data show that the TRPC3 channels play roles not commonly thought of for TRPC channels, i.e., ROS synthesis at the plasma membrane as a result of steady membrane stretching and ROS synthesis by mitochondria as a result of the uncoupling of the respiratory chain associated with Ca^{2+} overload.

H/R and I/R also caused activation of the NFATc3 transcription factor as seen by the decrease in the p-NFATc3/total NFATc3 (t-NFATc3) ratios, which we interpret as indicating the stimulation of its transcriptional activity reflected in the increase of TRPC3, TRPC6 (Figs. 3*A*, 3*C*, and 5*F*), and BAX (Figs. 2*B* and 5*F*). All aspects of I/R injury were ameliorated, when not prevented from occurring, by the ablation of the TRPC3/6/7 channels in I/R injury studies and by the nonselective pan-TRPC inhibitor SKF96365 in H/R injury studies using cultured cells.

Western blot analysis showed that both in H9c2 cells subjected to H/R and in AAR tissues the levels of TRPC3, TRPC6, BAX, and the α and β CaN subunits were augmented as compared with the corresponding controls (Figs. 3 and 5). In H9c2 cells the augmented levels of TRPC3 and TRPC6 were functionally active, as seen by the increased Ca^{2+} entry that could be evoked with the diacylglycerol agonist OAG (Fig. 3*B*). Preventing the increase in TRPCs by preventing p-NFATc dephosphorylation by the action of the CaM-stimulated CaN phosphatase (Fig. 5*F*) indicates that the increases in BAX and TRPC proteins are indeed the result of transcriptional activity resulting from p-NFATc3 dephosphorylation to NFATc3 and its migration to the nucleus. These observations are in agreement with observations in other systems published by Li et al. (59) showing that the transcription of BAX in renal podocytes is under the control of NFAT2; by Kuwahara et al. (31), who characterized NFATc3-binding sites in the 3′ regulatory region of the TRPC6 gene; and by Rosenberg et al. (44) showing TRPC1 transcription under the control of NFATc1 in skeletal muscle.

CaNα and CaNβ increased significantly after H/R in H9c2 cells (Fig. 2*E*) and in cardiac AAR tissue compared with sham-treated tissue (Fig. 5 *E*, *i*). We thus demonstrated that I/R-H/R leads to the activation of a positive-feedback signaling circuit in which the I/R-H/R induces Ca^{2+} entry through TRPCs, activating the Ca^{2+}→CaM→CaN→NFATc transcription program, which includes an increase in TRPC3 and TRPC6 channel protein (Fig. 3*C*) and function (Fig. 3*B*) and in turn leads to more Ca^{2+} entry.

Interruption of the positive-feedback circuit by inhibition of TRPCs with SKF96365 or genetic ablation of TRPC3 and TRPC6 resulted in protection against H/R-I/R–induced changes in p-AKT and p-GSK3β, which, in H9c2 myocytes were significantly increased over their levels in untreated control cells (Fig. 2*C*). It would seem that cells in culture are under some form of stress requiring a steady-state p-AKT enzyme acting as a survival kinase.

The available data indicate that the actual injury phase of H/R and I/R is the consequence of a complex proapoptotic reaction sequence that depends not only on increases in intercellular Ca^{2+} but also on the Ca^{2+}-independent (as far as is known) activation of Bcl2 homology 3 (BH3)-only members of the Bcl2 family of proteins, including Bad, in cardiomyocytes (57), which, by binding to Bcl2, release proapoptotic BAX [and BAK (Bcl2 antagonist/killer)]. BH3-only proteins are activated by stressing cells, as happens upon treatment with the kinase inhibitor staurosporine or with reacive oxygen species (ROS) such as H_2O_2. The likely I/R-H/R–generated activator of BH3-only proteins is superoxide radical ($O_2^{\cdot-}$) or its dismutated H_2O_2 produced by the activation of the plasma membrane-located Nox2. Recently, in maladaptive cardiac fibrosis, Nox2 was shown receive a positive protein–protein signaling input from TRPC3 triggered by steady hypertensive

stretching of cardiomyocytes (60). Because cells subjected to hypoxia swell (51), it is conceivable that there is not only Ca^{2+} entry but also formation of BH3-only–activating ROS as a consequence of I/R and H/R.

Unchecked, BAX (and BAK) molecules dissociate from Bcl2, oligomerize, and insert into the MOM where they assemble to form the BAX–BAK mitochondrial apoptosis channel (MAC) (61) (for reviews see Tait and Green, ref. 62, and Kinnally et al., ref. 63), through which Ca^{2+} fluxes into the intermembrane space and from there into the mitochondrial matrix carried by MCU and the mitochondrial TRPC3 channel, both resident in the mitochondrial inner membrane (MIM), leading to what is known as "mitochondrial Ca^{2+} overload." The Ca^{2+} overload uncouples the respiratory chain and leads to the generation of more superoxide and other ROS by mitochondrial Nox (e.g., Nox4) and other enzymes and to the assembly in the presence of matrix cyclophilin D (38) of the mPTP formed by aggregated VDAC proteins in the MOM and ANT molecules in the MIM. The mPTP collapses the trans-MIM ψm, as observed in H/R-treated cells (Fig. 2*A*), causing the release of cytochrome *c* from the intermembrane space face of the MIM, which exits through the MAC into the cytoplasm to associate with Apaf-1, triggering the caspase-activating chain that eventually will lead to cleaved caspase 3, as seen in H/R-I/R (Figs. 2*B* and 5*B*), and to apoptosis, as seen in AAR tissue (Fig. 5*A*). The matrix Ca^{2+} overload, mitochondrial ROS generation, and persistence of the mPTP cause mitochondrial swelling, rupture of the MOM, and necrotic cell death. At one point apoptotic and necrotic events are likely to coexist.

The finding reported here is the dependence of H/R and I/R injuries on the activity of TRPC channels. Before these studies, it had been established in both in vitro and in vivo studies that TRPC channels play key roles in participating in phenomena dependent on sustained signals such as cardiomyocyte growth (28), the development of cardiac hypertrophy (64, 65), and, more recently, in pathologic stretching-induced maladaptive cardiac fibrosis (60). Here we uncovered additional roles: the requirement for the inhibition of PI3K by an as yet unknown mechanism in cells and the activation of PI3K in intact tissue, the supply of Ca^{2+} to drive mitochondrial Ca^{2+} overload, the generation of ROS at the plasma membrane of swollen cardiomyocytes, and in an as yet undefined way, participating in the activation of BH3-only proteins conducive to apoptosis, perhaps by triggering Bad dephosphorylation to facilitate its interaction with antiapoptotic Bcl2 and directly or indirectly activating the BAX/BAK proteins to insert into the mitochondrial membrane.

Although the data presented here establish a role for TRPC channels in promoting Ca^{2+} overload, they do not prove that all the Ca^{2+} entry is carried by TRPCs. TRPCs are nonselective cation channels that allow the outward passage of K^+ and inward passage of Na^+ and Ca^{2+}. The monovalent cation movement promotes collapse of the plasma ψm and activation of reverse-mode exchange activity of NCX1, which thus also contributes to TRPC-dependent Ca^{2+} entry that sums to the direct TRPC-carried Ca^{2+} overload driving cell death. Likewise, the collapse of the plasma ψm activates voltage-gated Ca^{2+} channels (VGCCs) and Ca^{2+} entering through these channels also sums to the general TRPC-triggered Ca^{2+} overload and ensuing cell death. It remains for future studies to determine the proportion of Ca^{2+} entering through TRPCs vs. that entering through NCX1 and VGCCs. Also left for future studies is better establishing the mechanisms by which PI3K activity is regulated in H/R and I/R. Finally, we have not studied other factors that may contribute to I/R injury, especially changes that occur in SERCA2 activity as a consequence of the hypoxia/ischemia phase of H/R and I/R. As reported by Ronkainen et al. (66), SERCA2 is down-regulated by hypoxia, and this down-regulation is likely to facilitate injury caused by Ca^{2+} influx.

Materials and Methods

Sources of reagents and antibodies included the following: Fura2-AM (Invitrogen; F-1201), CPA (Sigma; C8031), SKF96365 (Sigma; S7809), thapsigargin (Invitrogen; T7459), LY294002 (Sigma; L9908), FBS (GIBCO; 16000–044), DMEM (Hyclone; SH30022.01), prestained protein standards (BioRad; 161-0374), PVDF membrane (Roche; 03010040001), protease inhibitor mixture (Roche; 11873580001), PMSF (Sigma; P7626), TUNEL assay (Roche; 11684817910), anti-TRPC3 (Alomone; ACC-016), anti-TRPC6 (Alomone; ACC-017), anti-TRPC1 (Alomone; ACC-010), anti-TRPC4 (Alomone; ACC-018), anti-calcineurin α (CaNα) (Protein Tech; 13422–1-AP), anti-CaNβ (Protein Tech; 13210–1-AP), anti-BAX (Cell Signaling; 2772), anti-BCL2 (Cell Signaling; 2876), anti-cleaved caspase 3 (Abcam; ab13847), anti–p-AKT(Ser473) (Cell Signaling; 4060P), anti–p-GSK3β (Ser9) (Cell Signaling; 5558P), anti–p-NFATc3(C-3, Ser240) (Santa Cruz; sc-365786), anti-NFAT3c (M-75) (Santa Cruz; sc-8321), and GAPDH (Abcam; ab9484). In addition anti-mouse TRPC3 (ab45/47affi; ab1144 affi) and anti-mouse TRPC6 (ab861 affi; ab1400 affi) used in Western blots were kindly provided by Veit Flockerzi from the Institute of Pharmacology and Toxicology, University of Saarland Medical School, Saarbrücken, Germany. These and all other chemicals, which were of the highest grade available, were used without further purification.

Primer sequences used in 35-cycle RT-PCR reactions are listed in Table S1.

Mice. TRPC3/6/7-deficient mice on a mixed C57BL/6J-129SvEv background were reconstituted from cryopreserved embryos at Charles River Laboratories. TRPC3/6/7 triple-KO parents were generated by crossing TRPC3-KO (67), TRPC6-KO (68), and TRPC7-KO (69) mice to the desired homozygosity at the Comparative Medicine Branch of the National Institute of Environmental Health Sciences, Research Triangle Park, NC (67, 70). Age-matched WT C57BL/6J-129SvEv mice, also reconstituted from frozen embryos at Charles River Laboratories, served as controls for the KO mice. Animals were treated in compliance with the *Guide for the Care and Use of Laboratory Animals* (National Academy of Sciences) (71). Animals were kept on a 12-h light–dark cycle in a temperature-controlled room with ad libitum access to food and water. All animal studies were approved by the Animal Care and Utilization Committee of Huazhong University of Science and Technology. Anesthetic procedures were used to ensure that animals not suffer unduly during and after the experimental procedures.

In Vivo I/R: Mouse Model of I/R Injury. Eight- to twelve-week-old TRPC3/6/7$^{-/-}$ and WT male mice were anesthetized with 3.3% (wt/vol) chloral hydrate (Sigma; 231000) and were placed in a supine position on a heating pad (37 °C). Animals were intubated with a 20G stump needle and were ventilated with room air with the use of a MiniVent mouse ventilator. Following left thoracotomy located between the third and fourth ribs, the left anterior descending coronary artery was visualized under a dissecting microscope (Leica) and ligated by a sterile 8–0 Prolene suture. A suture was placed around the coronary artery 2 mm below the left atrium and was passed through a snare. The left coronary artery was ligated by tying off the snare. Proper ligation was confirmed by visual observation of the left ventricle wall turning pale. After 30 min of regional ischemia, the heart was allowed to reperfuse (removal of the snare and suturing the incision), leading to loss of the discoloration of the myocardium distal to the occlusion. Sham-operated animals underwent the same procedure without occlusion of the left anterior descending coronary artery. All procedures were approved by the Huazhong University of Science and Technology's Center of Institutional Animal Care and Use Committee.

Infarct Size. After a 24-h reperfusion period, the animals were reanesthetized, the heart was arrested at the diastolic phase by injection of KCl (20 mM), and the left anterior descending coronary artery was occluded again. To demarcate the ischemic AAR, the ascending aorta was cannulated in reverse sense, and 0.2 mL of 1% (wt/vol) Evans blue was perfused into the coronary arteries. The heart was excised immediately and cut into 1-mm-thick slices perpendicular to the long axis of the heart from the apex (typically, five slices per heart). The left ventricle was counterstained with 1% (wt/vol) 2,3,5-triphenyltetrazolium chloride (TTC; Sigma) at 37 °C for 15 min. Images were analyzed by Image-Pro Plus (Media Cybernetics). To determine left ventricle AAR and IS after I/R, the pale areas (IS), the blue areas (area not at risk, ANAR), and not-blue areas (AAR) were measured, and the percentage of IS/(AAR+ANAR) and AAR/(AAR+ANAR) were calculated.

Animals subjected to 30-min/24-h I/R were anesthetized and heparinized intravenously. Hearts were perfused with 10% (wt/vol) buffered formalin, dissected, washed, and weighed. The fixed heart tissues were dehydrated and embedded in paraffin, longitudinally sectioned at 5-μm thickness, and used to prepare histology tissue slides, which then were stained with H&E. Whole-section images were taken, and Image-Pro Plus software was used to perform histology analysis.

Primary Culture of Neonatal Mouse Ventricular Myocytes. Neonatal (0- to 1-d-old) mice were rinsed quickly in 75% (vol/vol) ethanol for surface sterilization. Hearts of the pups were dissected and washed with Ca^{2+}/Mg^{2+}-free D-Hanks solution [in mmol/L: NaCl 137, KCl 5.4, Na_2HPO_4 0.12, H_2O 0.35, KH_2PO_4 0.4, $NaHCO_3$ 4.2, and glucose 5.6 (pH 7.4)] and then were minced into small pieces ~1 mm^3 and

digested with 5 mL of 0.03% trypsin for 5 min at 37 °C. The supernatant was discarded; the resulting pellets were resuspended with fresh Ca^{2+}/Mg^{2+}-free D-Hanks solution containing 0.1% collagenase II (Worthington; LS004176) and were kept at 37 °C in a water bath with mild agitation for 5 min. Then agitation was stopped for an additional 2 min. The supernatants were collected, transferred into a new tub, mixed with same volume of DMEM containing 10% (vol/vol) FCS (to stop collagenase II digestion). This collagenase II digestion step was repeated another four times. Cells collected in each cycle were filtered with a Becton-Dickinson Falcon 100-μm cell strainer followed by brief sedimentation at 150 × *g*. The final pellets were resuspended in 10 mL of culture medium [high-glucose DMEM (Gibco) supplemented with 5% (vol/vol) FCS, 100 IU/mL of penicillin, and 100 μg/mL of streptomycin] and were seeded into 100-mm tissue-culture dishes and cultured for 2 h. Unattached cardiomyocytes were collected by brief centrifugation at 100 × *g* for 5 min. The resulting pellets were resuspended in DMEM with 5% (vol/vol) FCS and 0.1 μmol/L BrdU (Sigma-Aldrich), seeded onto round coverslips (20 mm in diameter) precleaned in cleaning solution composed by volume of one part 6.3% (wt/vol) $K_2Cr_2O_7$/4 parts of H_2SO_4, and then with ethanol, flamed and coated with 0.1 mg/mL poly-L-lysine (Sigma; P1399), placed in 12-well plates at a density of 5×10^5 cells/mL (1 mL per well), and cultured in 95% air, 5% CO_2 at 37 °C for 4–6 d before they were tested for thapsigargin-evoked Ca^{2+} entry (SOCE) or OAG-stimulated Ca^{2+} entry.

In Vitro H/R Experiments. To simulate in vivo myocardial I/R injury in vitro, H9c2 rat cardiomyoblasts were subjected to H/R. Hypoxia [partial pressure of oxygen (PO_2) <10 mmHg] was achieved by placing cardiomyocyte cells into an hypoxic incubator (atmosphere of 5% CO_2 and 95% N_2) in serum-free/glucose-free Hepes-buffered medium (in millimoles per liter: NaH_2PO_4 0.9, $NaHCO_3$ 6.0, $CaCl_2$ 1.0, $MgSO_4$ 1.2, sodium lactate 40, Hepes 20, NaCl 98.5, KCl 10, pH 6.8) at 37 °C. Reoxygenation was achieved by transferring the cells to normoxic H9c2 culture medium [DMEM (high glucose) supplemented with 10% (vol/vol) FCS, 100 IU/mL of penicillin and 100 μg/mL of streptomycin] and incubation in 95% air, 5% CO_2 to simulate reperfusion. Cells were subjected to 9 h hypoxia to simulate ischemia and 6 h reoxygenation to simulate reperfusion. Cells incubated in normoxic H9c2 culture medium were prepared in parallel for each condition and served as controls.

Ca^{2+} Entry Measurements. H9c2 rat cardiomyoblasts were seeded onto uncoated coverslips 30 h before the test for TRPC-mediated Ca^{2+} entry. Nine hours before the test cells were subjected to the 9-h H/R protocol and were brought into a normoxic environment. Coverslips with H9c2 cells or cultured neonatal cardiomyocytes were loaded with 2 μM Fura2-AM (Molecular Probes) for 30 min at room temperature in serum-free Opti-MEM (Gibco). The coverslips were mounted onto the platform of an inverted epifluorescence microscope. To measure thapsigargin-evoked Ca^{2+} entry, cells were bathed in sequence with 2 mM Ca^{2+} in HPSS (in millimoles per liter: NaCl 140, KCl 5, $MgCl_2$ 1, glucose 10, and Hepes 10, pH 7.4), 50 μM EGTA in HPSS for 2 min, 50 μM EGTA and 2 μM thapsigargin in HPSS for 10 min, and 2 mM Ca^{2+} plus 2 μM thapsigargin in HPSS, as shown in the figures. Ca^{2+} entry also was assessed with or without the TRPC inhibitor SKF96365 (5 μM) and without store depletion. For DAG-stimulated Ca^{2+} entry, cells were bathed in sequence in HPSS with 2 mM Ca^{2+} for 2 min, HPSS without Ca^{2+} for 2 min, HPSS plus 10 μM OAG for 2 min, and finally in HPSS plus 10 μM OAG and 2 mM Ca^{2+}, as indicated in Fig. 3*B*. Cytosolic Ca^{2+} was monitored with an Olympus IX51 inverted fluorescence microscope and SlideBook software, using excitation wavelengths of 340 and 380 nm to detect Fura-2/Fura2-Ca^{2+} fluorescence emissions at 510 nm (20).

TUNEL Assays. TUNEL assays were performed according to the manufacturer's instructions (Roche). In brief, after 24 h of reperfusion, the AAR was removed from hearts fixed in 3.7% (wt/vol) buffered formaldehyde and embedded in paraffin. Five-micrometer-thick tissue sections were deparaffinized, rehydrated, and rinsed with PBS for 10 min. A positive control sample was prepared from a normal heart section by treatment with DNase I (10 U/mL) for 10 min at room temperature. The sections were pretreated with 0.1% Triton X-100 and 0.1% (wt/vol) sodium citrate for 8 min at room temperature and were washed with Tris-buffered saline (TBS; 20 mM Tris·HCl, 137 mM NaCl, pH 7.4). The slices were blocked with 3% (wt/vol) BSA and 20% (vol/vol) FCS for 30 min at room temperature and were subjected to reaction with terminal deoxynucleotidyl transferase (TdT) enzyme and Alexa Fluor 488-conjugated dUTP (Roche; 11684817910) at 37 °C for 1 h. Nuclei were stained with DAPI (Roche, 216276) for 10 min. The sections were inspected with a confocal microscope (Olympus FV1000). Six slices per group were prepared, and 10 different regions were observed in each section. The results were analyzed with Image-Pro Plus software.

Electron Microscopy. Briefly, after 24 h of reperfusion, a small (1-mm^3) piece of AAR was removed from the hearts and quickly fixed with 2.5% (wt/vol) glutaraldehyde in 0.1 mol/L cacodylate buffer for 2 h, postfixed in 2% (wt/vol) OsO_4 in 0.1 mol/L cacodylate buffer for 1 h, and embedded in LX-112 (Ladd Research). Sections were stained with uranyl acetate and lead citrate and were observed with an HT7700 Hitachi electron microscope (Hitachi Limited). Random sections were taken by an electron microscopy technician blinded to sample information.

In Vivo Functional Analysis. Echocardiography (ECHO) was performed with a Vevo1100 imaging system and a MS400 transducer, which is designed specifically for mice and rats (VisualSonics). After the I/R procedure, mice were anesthetized with 2% (vol/vol) isoflurane during the ECHO procedure. Hearts were viewed in the short axis between the two papillary muscles and analyzed in M-mode. Parameters were measured offline (Vevo software) including end-diastolic diameter, end-systolic diameter, posterior wall thickness, and septal wall thickness to determine cardiac morphological changes and EF, heart rate, and FS.

Measurement of Mitochondrial ψm. To measure mitochondrial ψm, cardiomyocytes were exposed to 9-h/6-h H/R. Cells were washed with PBS (1×PBS: 137 mM NaCl, 2.7 mM KCl, 0.12 mM Na_2HPO_4, 10 mM H_2O, 2 mM KH_2PO_4) and were incubated with JC-1 (Beyotime Biotechnology) at 37 °C for 20 min in the dark. After incubation with the dye, the plates were washed three times with HPSS. Fluorescence was measured first at excitation/emission 485/580 nm (red) and then at excitation/emission 485/530 nm (green) using an EnVision plate reader (Perkin-Elmer). The results were analyzed with Image-Pro Plus software.

Immunoblots. For immunoblots of cardiac tissue, 100 mg AAR were lysed in 1 mL 50 mM Tris (pH 7.4), 150 mM NaCl, 1% Triton X-100, 1% sodium deoxycholate, 0.1% SDS, 1 mM PMSF, and 1× Roche antiprotease mixture. Cells on a 100-mm dish (~10×10^6 cells) were rinsed with PBS, overlaid with 1 mL lysis buffer [50 mM Tris·HCl (pH 7.4), 150 mM NaCl, 0.1% SDS, 1% Nonidet P-40, 1 mM EDTA] containing 1 mM PMSF and 1× Roche antiprotease mixture, and were scraped and homogenized with an ultrasonic cell disruptor. Proteins in tissue and cell lysates were separated by SDS/PAGE with 12% (wt/vol) or 8% (wt/vol) precast polyacrylamide gels (Invitrogen) and were transferred to PVDF membranes by electroelution. Membranes were cut into horizontal strips with the protein band of interest estimated on the basis of comigrating prestained protein standards, blocked in TBS and Tween 20 [20 mM Tris·HCl (pH 7.4), 140 mM NaCl, 0.05% Tween-20) containing 4% (wt/vol) BSA, and were exposed to primary antibodies overnight at 4 °C. The following kDa values were used: BAX, 21; Bcl2, 26; cleaved caspase 3, 17; p-AKT and total AKT (t-AKT), 60; p-GSK3β and total GSK3β (t-GSK3β), 46; p-NFATc3, 130, t-NFATc3, 120–135; TRPC3, 97; TRPC4, 112; TRPC6, 106; CaNα, 61; CaNβ, 19, GAPDH, 36. Blots were visualized using secondary antibodies conjugated with HRP from Santa Cruz Biotechnology and enhanced chemiluminescence reagents from GE Healthcare.

Statistical Analysis. Data analysis was performed by observers blinded to experimental groups. All data are expressed as means ± SEM. Statistical analysis was performed with Prism 4.0 (GraphPad) by the unpaired Student *t* test or one-way ANOVA followed by a post hoc test with Bonferroni correction for multiple comparisons. Statistical significance was defined as $P < 0.05$.

ACKNOWLEDGMENTS. This research was supported by National Natural Science Foundation of China Grants 31171087 and 30970662 (to Y.L.), and NIH Intramural Research Program Project Z01-ES-101684 (L.B.).

1. Murphy E, Steenbergen C (2008) Mechanisms underlying acute protection from cardiac ischemia-reperfusion injury. *Physiol Rev* 88(2):581–609.
2. Halestrap AP (2006) Calcium, mitochondria and reperfusion injury: A pore way to die. *Biochem Soc Trans* 34(Pt 2):232–237.
3. Klein HH, et al. (1989) Treatment of reperfusion injury with intracoronary calcium channel antagonists and reduced coronary free calcium concentration in regionally ischemic, reperfused porcine hearts. *J Am Coll Cardiol* 13(6):1395–1401.
4. Boden WE, et al. (2000) Diltiazem in acute myocardial infarction treated with thrombolytic agents: A randomised placebo-controlled trial. Incomplete Infarction Trial of European Research Collaborators Evaluating Prognosis post-Thrombolysis (INTERCEPT). *Lancet* 355(9217):1751–1756.
5. Dietrich A, et al. (2007) In vivo TRPC functions in the cardiopulmonary vasculature. *Cell Calcium* 42(2):233–244.
6. Ghali JK, et al. (2007) A phase 1-2 dose-escalating study evaluating the safety and tolerability of istaroxime and specific effects on electrocardiographic and hemodynamic

parameters in patients with chronic heart failure with reduced systolic function. *Am J Cardiol* 99(2A, 2a):47A–56A.
7. Micheletti R, et al. (2007) Istaroxime, a stimulator of sarcoplasmic reticulum calcium adenosine triphosphatase isoform 2a activity, as a novel therapeutic approach to heart failure. *Am J Cardiol* 99(2A, 2a):24A–32A.
8. Putney JW, Jr, Broad LM, Braun FJ, Lievremont JP, Bird GS (2001) Mechanisms of capacitative calcium entry. *J Cell Sci* 114(Pt 12):2223–2229.
9. Arakawa N, et al. (2000) KB-R7943 inhibits store-operated Ca(2+) entry in cultured neurons and astrocytes. *Biochem Biophys Res Commun* 279(2):354–357.
10. Kurebayashi N, Ogawa Y (2001) Depletion of Ca^{2+} in the sarcoplasmic reticulum stimulates Ca^{2+} entry into mouse skeletal muscle fibres. *J Physiol* 533(Pt 1):185–199.
11. Pang Y, Hunton DL, Bounelis P, Marchase RB (2002) Hyperglycemia inhibits capacitative calcium entry and hypertrophy in neonatal cardiomyocytes. *Diabetes* 51(12): 3461–3467.
12. Trepakova ES, et al. (2000) Calcium influx factor directly activates store-operated cation channels in vascular smooth muscle cells. *J Biol Chem* 275(34):26158–26163.
13. Zhang SL, et al. (2011) Mutations in Orai1 transmembrane segment 1 cause STIM1-independent activation of Orai1 channels at glycine 98 and channel closure at arginine 91. *Proc Natl Acad Sci USA* 108(43):17838–17843.
14. Feske S, et al. (2006) A mutation in Orai1 causes immune deficiency by abrogating CRAC channel function. *Nature* 441(7090):179–185.
15. Vig M, et al. (2006) CRACM1 is a plasma membrane protein essential for store-operated Ca^{2+} entry. *Science* 312(5777):1220–1223.
16. Zhu X, et al. (1996) trp, a novel mammalian gene family essential for agonist-activated capacitative Ca^{2+} entry. *Cell* 85(5):661–671.
17. Zitt C, et al. (1996) Cloning and functional expression of a human Ca^{2+}-permeable cation channel activated by calcium store depletion. *Neuron* 16(6):1189–1196.
18. Kim MS, et al. (2009) Native store-operated Ca^{2+} influx requires the channel function of Orai1 and TRPC1. *J Biol Chem* 284(15):9733–9741.
19. Asanov A, et al. (2015) Combined single channel and single molecule detection identifies subunit composition of STIM1-activated transient receptor potential canonical (TRPC) channels. *Cell Calcium* 57(1):1–13.
20. Warnat J, Philipp S, Zimmer S, Flockerzi V, Cavalié A (1999) Phenotype of a recombinant store-operated channel: Highly selective permeation of Ca^{2+}. *J Physiol* 518(Pt 3):631–638.
21. Freichel M, et al. (2001) Lack of an endothelial store-operated Ca^{2+} current impairs agonist-dependent vasorelaxation in TRP4-/- mice. *Nat Cell Biol* 3(2):121–127.
22. Philipp S, et al. (1998) A novel capacitative calcium entry channel expressed in excitable cells. *EMBO J* 17(15):4274–4282.
23. Liao Y, et al. (2009) A role for Orai in TRPC-mediated Ca^{2+} entry suggests that a TRPC: Orai complex may mediate store and receptor operated Ca^{2+} entry. *Proc Natl Acad Sci USA* 106(9):3202–3206.
24. Liao Y, et al. (2008) Functional interactions among Orai1, TRPCs, and STIM1 suggest a STIM-regulated heteromeric Orai/TRPC model for SOCE/Icrac channels. *Proc Natl Acad Sci USA* 105(8):2895–2900.
25. Liao Y, et al. (2007) Orai proteins interact with TRPC channels and confer responsiveness to store depletion. *Proc Natl Acad Sci USA* 104(11):4682–4687.
26. Yuan JP, et al. (2009) SOAR and the polybasic STIM1 domains gate and regulate Orai channels. *Nat Cell Biol* 11(3):337–343.
27. Eder P, Molkentin JD (2011) TRPC channels as effectors of cardiac hypertrophy. *Circ Res* 108(2):265–272.
28. Onohara N, et al. (2006) TRPC3 and TRPC6 are essential for angiotensin II-induced cardiac hypertrophy. *EMBO J* 25(22):5305–5316.
29. Nakayama H, Wilkin BJ, Bodi I, Molkentin JD (2006) Calcineurin-dependent cardiomyopathy is activated by TRPC in the adult mouse heart. *FASEB J* 20(10):1660–1670.
30. Bush EW, et al. (2006) Canonical transient receptor potential channels promote cardiomyocyte hypertrophy through activation of calcineurin signaling. *J Biol Chem* 281(44):33487–33496.
31. Kuwahara K, et al. (2006) TRPC6 fulfills a calcineurin signaling circuit during pathologic cardiac remodeling. *J Clin Invest* 116(12):3114–3126.
32. Seth M, et al. (2009) TRPC1 channels are critical for hypertrophic signaling in the heart. *Circ Res* 105(10):1023–1030.
33. Ohba T, et al. (2007) Upregulation of TRPC1 in the development of cardiac hypertrophy. *J Mol Cell Cardiol* 42(3):498–507.
34. Wu X, Eder P, Chang B, Molkentin JD (2010) TRPC channels are necessary mediators of pathologic cardiac hypertrophy. *Proc Natl Acad Sci USA* 107(15):7000–7005.
35. Makarewich CA, et al. (2014) Transient receptor potential channels contribute to pathological structural and functional remodeling after myocardial infarction. *Circ Res* 115(6):567–580.
36. Kimes BW, Brandt BL (1976) Properties of a clonal muscle cell line from rat heart. *Exp Cell Res* 98(2):367–381.
37. Soboloff J, et al. (2006) Orai1 and STIM reconstitute store-operated calcium channel function. *J Biol Chem* 281(30):20661–20665.
38. Baines CP, et al. (2005) Loss of cyclophilin D reveals a critical role for mitochondrial permeability transition in cell death. *Nature* 434(7033):658–662.
39. Molkentin JD, et al. (1998) A calcineurin-dependent transcriptional pathway for cardiac hypertrophy. *Cell* 93(2):215–228.
40. Macián F, López-Rodríguez C, Rao A (2001) Partners in transcription: NFAT and AP-1. *Oncogene* 20(19):2476–2489.
41. Cortés R, et al. (2012) Differences in MEF2 and NFAT transcriptional pathways according to human heart failure aetiology. *PLoS One* 7(2):e30915.
42. Hogan PG, Chen L, Nardone J, Rao A (2003) Transcriptional regulation by calcium, calcineurin, and NFAT. *Genes Dev* 17(18):2205–2232.
43. Wilkins BJ, et al. (2002) Targeted disruption of NFATc3, but not NFATc4, reveals an intrinsic defect in calcineurin-mediated cardiac hypertrophic growth. *Mol Cell Biol* 22(21):7603–7613.
44. Rosenberg P, et al. (2004) TRPC3 channels confer cellular memory of recent neuromuscular activity. *Proc Natl Acad Sci USA* 101(25):9387–9392.
45. Frost RJ, Olson EN (2010) Separating the good and evil of cardiac growth by CIB1 and calcineurin. *Cell Metab* 12(3):205–206.
46. Noguchi H, et al. (2004) A new cell-permeable peptide allows successful allogeneic islet transplantation in mice. *Nat Med* 10(3):305–309.
47. Dejean LM, et al. (2005) Oligomeric Bax is a component of the putative cytochrome c release channel MAC, mitochondrial apoptosis-induced channel. *Mol Biol Cell* 16(5): 2424–2432.
48. Lakshmikuttyamma A, et al. (2003) Activation of calcineurin expression in ischemia-reperfused rat heart and in human ischemic myocardium. *J Cell Biochem* 90(5): 987–997.
49. Joshi S, Wei J, Bishopric NH (2016) A cardiac myocyte-restricted Lin28/let-7 regulatory axis promotes hypoxia-mediated apoptosis by inducing the AKT signaling suppressor PIK3IP1. *Biochim Biophys Acta* 1862(2):240–251.
50. Zhu Z, et al. (2007) PI3K is negatively regulated by PIK3IP1, a novel p110 interacting protein. *Biochem Biophys Res Commun* 358(1):66–72.
51. Gores GJ, et al. (1989) Swelling, reductive stress, and cell death during chemical hypoxia in hepatocytes. *Am J Physiol* 257(2 Pt 1):C347–C354.
52. Chaudhuri P, et al. (2016) Membrane translocation of TRPC6 channels and endothelial migration are regulated by calmodulin and PI3 kinase activation. *Proc Natl Acad Sci USA* 113(8):2110–2115.
53. Joyal JL, et al. (1997) Calmodulin activates phosphatidylinositol 3-kinase. *J Biol Chem* 272(45):28183–28186.
54. Datta SR, et al. (1997) Akt phosphorylation of BAD couples survival signals to the cell-intrinsic death machinery. *Cell* 91(2):231–241.
55. Datta SR, et al. (2000) 14-3-3 proteins and survival kinases cooperate to inactivate BAD by BH3 domain phosphorylation. *Mol Cell* 6(1):41–51.
56. Gardai SJ, et al. (2004) Phosphorylation of Bax Ser184 by Akt regulates its activity and apoptosis in neutrophils. *J Biol Chem* 279(20):21085–21095.
57. Wang W, Peng Y, Wang Y, Zhao X, Yuan Z (2009) Anti-apoptotic effect of heat shock protein 90 on hypoxia-mediated cardiomyocyte damage is mediated via the phosphatidylinositol 3-kinase/AKT pathway. *Clin Exp Pharmacol Physiol* 36(9):899–903.
58. Feng S, et al. (2013) Canonical transient receptor potential 3 channels regulate mitochondrial calcium uptake. *Proc Natl Acad Sci USA* 110(27):11011–11016.
59. Li R, et al. (2013) NFAT2 mediates high glucose-induced glomerular podocyte apoptosis through increased Bax expression. *Exp Cell Res* 319(7):992–1000.
60. Kitajima N, et al. (2016) TRPC3 positively regulates reactive oxygen species driving maladaptive cardiac remodeling. *Sci Rep* 6:37001.
61. Wei MC, et al. (2001) Proapoptotic BAX and BAK: A requisite gateway to mitochondrial dysfunction and death. *Science* 292(5517):727–730.
62. Tait SW, Green DR (2010) Mitochondria and cell death: Outer membrane permeabilization and beyond. *Nat Rev Mol Cell Biol* 11(9):621–632.
63. Kinnally KW, Peixoto PM, Ryu SY, Dejean LM (2011) Is mPTP the gatekeeper for necrosis, apoptosis, or both? *Biochim Biophys Acta* 1813(4):616–622.
64. Seo K, et al. (2014) Combined TRPC3 and TRPC6 blockade by selective small-molecule or genetic deletion inhibits pathological cardiac hypertrophy. *Proc Natl Acad Sci USA* 111(4):1551–1556.
65. Camacho Londoño JE, et al. (2015) A background Ca^{2+} entry pathway mediated by TRPC1/TRPC4 is critical for development of pathological cardiac remodelling. *Eur Heart J* 36(33):2257–2266.
66. Ronkainen VP, Skoumal R, Tavi P (2011) Hypoxia and HIF-1 suppress SERCA2a expression in embryonic cardiac myocytes through two interdependent hypoxia response elements. *J Mol Cell Cardiol* 50(6):1008–1016.
67. Hartmann J, et al. (2008) TRPC3 channels are required for synaptic transmission and motor coordination. *Neuron* 59(3):392–398.
68. Domes K, et al. (2015) Murine cardiac growth, TRPC channels, and cGMP kinase I. *Pflugers Arch* 467(10):2229–2234.
69. Perez-Leighton CE, Schmidt TM, Abramowitz J, Birnbaumer L, Kofuji P (2011) Intrinsic phototransduction persists in melanopsin-expressing ganglion cells lacking diacylglycerol-sensitive TRPC subunits. *Eur J Neurosci* 33(5):856–867.
70. Dietrich A, et al. (2005) Increased vascular smooth muscle contractility in TRPC6-/- mice. *Mol Cell Biol* 25(16):6980–6989.
71. National Research Council (2011) Guide for the Care and Use of Laboratory Animal. (National Academies Press, Washington, DC), 8th Ed.